J Mater Sci (2020) 55:5655–5666

Polymers & biopolymers

Electrospun cyclodextrin nanofibers as precursor for carbon nanofibers

Bhushan Patil[1,*], Zehra Irem Yildiz[1], and Tamer Uyar[1,2,*]

[1] Institute of Materials Science and Nanotechnology, Bilkent University, Ankara 06800, Turkey
[2] Department of Fiber Science and Apparel Design, College of Human Ecology, Cornell University, Ithaca, NY 14853, USA

Received: 15 September 2019
Accepted: 17 January 2020
Published online:
27 January 2020

ABSTRACT

The carbon nanofibers (CNF) based on the electrospun polymer-free hydroxypropyl-β-cyclodextrin (HPβCD) nanofibers were obtained by the combination of chemical and thermal (pyrolysis) treatment. The thermal and chemical decomposition of HPβCD makes it challenging to obtain persistent CNF from HPβCD nanofibers. The chemical treatment of HPβCD nanofibers by using 0.6 mM H_2SO_4 partially dissolves nanofibers and resulted in fused CNF while direct pyrolysis of HPβCD nanofibers totally ruins the nanofiber structure and produces char. The partial chemical treatment of HPβCD nanofibers with 10 μM H_2SO_4 dehydrates the top layer of the nanofibers, and a shield-like structure is formed which helps to retain the fibrous morphology during the pyrolysis. The diameter of HPβCD nanofibers was reduced after carbonization process where CNF having average diameter of 380 ± 150 nm were obtained. The presence of typical D and G Raman bands and XRD peak at $2\theta \sim 26°$ further validates CNF formation from HPβCD nanofibers. The oxygen content is decreased from 34.7 to 5.8%, and carbon content increased from 62.3% to 94.2% after transformation of HPβCD nanofibers into CNF. To the best of our knowledge, for the first time, this study reports the use of electrospun polymer-free HPβCD nanofibers as a precursor to produce CNF.

Introduction

Carbon is of an interesting element due to its transformable properties by controlling the allotropes such as graphite, fullerenes, graphene, carbon nanotube, and diamond [1]. The carbon materials exist in various dimensions such as zero-dimensional (i.e., quantum dots), one-dimensional (i.e., carbon nanotubes, carbon fibers), and two-dimensional (i.e., graphene) [2] having different conductivity [3, 4], optical properties [5], thermal properties [6], and mechanical properties [7]. Nanostructure forms of carbon have numerous applications in the energy [8, 9], sensors [10], biomedical [11], aeronautics [12], electronics [3], and environmental [13] fields. Among the different structural form of carbon, carbon fibers (CF) and carbon nanofibers (CNF) are quite attractive due to their easy fabrication and controllable

Address correspondence to E-mail: bhushanpatil25@gmail.com; tu46@cornell.edu

https://doi.org/10.1007/s10853-020-04374-3

properties [14]. CF are commonly produced from polymeric precursor such as polyacrylonitrile (PAN) fibers [15] yet the use of more economical synthetic precursor such as polyethylene fibers [16] is also possible. CF can also be produced from bio-based precursors such as regenerated cellulose fibers (i.e., rayon) and lignin-based fibers [17, 18]. Similar to CF, CNF are produced by pyrolysis of precursor nanofibers in which nanofibers are typically obtained by electrospinning technique or some other nanofiber production techniques. The electrospinning is a versatile fiber production technique to produce ultrafine fibers (nanofibers) having fiber diameter less than one micron [19]. Electrospun nanofibers obtained from a variety of different materials such as PAN [20], polyvinylidene fluoride (PVDF) [21], polymer of intrinsic porosity (PIM-1) [22], and lignin [23] have been used as precursors for the production of CNF [24]. In most cases, toxic organic solvents are used for the electrospinning of fibers; for instance, dimethylformamide (DMF) is used for the synthesis of electrospun PAN fibers. There is a growing interest to use bio-based materials into suitable precursor fibers for the production of CF and CNF [18, 25]. In this study, we aimed to produce CNF from electrospun cyclodextrin nanofibers. This is also a green approach since water is used as a solvent for the electrospinning of cyclodextrin nanofibers.

Cyclodextrins (CD) are bio-based molecules formed by the enzymatic modification of starch which are categorized as cyclic oligosaccharides. The native cyclodextrins are mainly named as α-CD (6 units), β-CD (7 units), and γ-CD (8 units) based on the number of α-D-glucopyranoside units linked by α-1,4-glycosidic bonds in a ring shape [26]. Besides these native cyclodextrins, chemically modified cyclodextrins such as hydroxyl propylated CD, methylated CD, and sulfobutylated CD are also available in which these modified cyclodextrins are more hydrophilic in nature and therefore highly water soluble [27]. CD molecules form aggregates in their concentrated solutions due to intermolecular hydrogen bonding, and the presence of such aggregates facilitates the electrospinning of nanofibers from CD solutions [28]. Even though the electrospinning of nanofibers from cyclodextrins is much more challenging than electrospinning of nanofibers from polymeric materials since cyclodextrins are small molecules, electrospinning of nanofibers from chemically modified CD molecules (i.e., hydroxypropylated CD [29–31], methylated CD [30, 32], and sulfobutylated CD [33–35]) is relatively easy compared to native CD molecules (i.e., α-CD [36, 37], β-CD [36–38], and γ-CD [36, 39]).

Being cyclic oligosaccharides, CD molecules can be used precursor for carbon materials [40]. Thermal decomposition of CD molecules leads to char or pyran and furan production similar to cellulose [41]. The typical thermal decomposition of CD molecules involves two steps; at low temperature, char is produced by glycosidic-bond cleavage with chain-end mechanism, and after that, pyran and furan are produced mainly by transglycosylation and glycolysis process via intra-chain cleavage at higher temperatures [42]. Thus, maintaining the structure during the pyrolysis is a great challenge for CD-based carbon products. In addition to pyrolysis, chemical decomposition of CD has been reported by the dehydration; however, this chemical acidic treatment destroys the CD structure while producing carbon [40]. On the other hand, pyrolysis of CD-based nanosponges where the CD molecules were hyper cross-linked with the pyromellitic dianhydride resulted in hollow spheres of microporous carbon, whereas CD cross-linked with hexamethylene diisocyanate was ineffective to produce microporous carbon demonstrating that the cross-linker drastically influences the carbon properties particularly surface area and porosity of the CD-based carbons [43]. It has also been reported that microfibers of microporous carbon could be obtained by pyrolysis from electrospun fibrous nanosponges of cyclodextrin polymer cross-linked with pyromellitic dianhydride [44]. Yet, to the best of our knowledge, there has been no study reported related to the use of electrospun polymer-free pure cyclodextrin nanofibers as a precursor for obtaining the carbon nanofibers. Thus, in the present study, pure CD electrospun nanofibers were used as the precursor for the production CNF. Hydroxypropyl-β-cyclodextrin (HPβCD) nanofibers were successfully produced in the form of self-standing nanofibrous nonwoven mat without the polymeric support or cross-linker by electrospinning [30]. Furthermore, to overcome complete char formation or total decomposition of CD and to maintain fibrous structure of electrospun HPβCD nanofibers, we have optimized combination of chemical and thermal treatment to obtain CD-based CNF. The novelty of the present study is the carbonization of electrospun polymer-free HPβCD nanofibers by the dehydration

(chemical treatment) and pyrolysis (thermal treatment) in order to obtain CNF.

Experimental

Electrospinning of HPβCD nanofibers

The electrospinning of pristine HPβCD nanofibers without using any carrier polymeric matrix was performed according to our previous study [30]. A highly concentrated aqueous solution of HPβCD (Cavasol® W7 HP, kindly given by Wacker Chemie AG, Germany) at a concentration of 200%, w/v (2 g of HPβCD in 1 mL solvent) was prepared in water (Millipore Milli-Q). After that, the electrospinning of the 200% (w/v) HPβCD aqueous solution was performed in order to produce HPβCD nanofibers. For the electrospinning of the HPβCD nanofibers, the 200% (w/v) HPβCD aqueous solution was loaded into 1 mL plastic syringe with a 27-gauge metallic needle. Then, the syringe loaded with 200% (w/v) HPβCD aqueous solution was placed on a syringe pump (KD Scientific, KDS-101, USA), and the flow rate of 0.5 mL h^{-1} was set for the HPβCD solution. The electrospinning was performed at a high voltage of 15 kV by using high voltage–power supply (AU Series, Matsusada Precision Inc., Japan). The distance between the stationary grounded metal collector covered with aluminum foil and the tip of the needle was adjusted as ~ 15 cm. The electrospun HPβCD nanofibers were deposited on the collector in the form of a nonwoven mat. The electrospinning was carried out in an enclosed Plexiglas box at 25 °C and 30% relative humidity.

Carbonization

The carbonization of electrospun HPβCD nanofibrous mat was carried out in two ways: first by chemical dehydration and second by the combination of chemical and thermal (pyrolysis) treatments. Prior to carbonization, the electrospun HPβCD nanofibrous mat was vacuum dried at 120 °C for 24 h.

First method: chemical dehydration of electrospun HPβCD nanofibers

The electrospun HPβCD nanofibers were chemically dehydrated by slightly altering the procedure reported for the synthesis of carbon from the β-CD [40]. Unlike reported acid concentration (i.e., 0.6 M H_2SO_4), the concentration of H_2SO_4 was reduced to 0.6 mM to avoid complete dehydration of HPβCD nanofibers. In the flask, totally 30 mL solution of 0.6 mM H_2SO_4 (Sigma-Aldrich, 99.9%) was prepared in the toluene (Sigma-Aldrich, anhydrous 99.8%). About 33 mg of HPβCD nanofibrous mat was immersed in the flask containing 0.6 mM H_2SO_4 and fixed it with the reflux system. The system was refluxed at 110 °C for 24 h, and the stirring of the solution was circumvented to avoid the damage of the HPβCD nanofibrous mat by mechanical forces. The HPβCD nanofibrous mat slowly turns yellow after approximately 10-h reflux and then finally becomes black after 24-h reflux. An excess solution was decanted from the flask leaving behind the wet CNF. The wet CNF were further dried by the rotary evaporator to remove the remaining solvent. After that, the chemically dehydrated HPβCD nanofibrous mat was thoroughly washed with the deionized water. The untreated HPβCD nanofibers can be rapidly dissolved in the water and washed away during this step leaving behind the chemically treated carbon nanofibers. The CNF obtained from the chemical dehydration process of HPβCD nanofibers by using 0.6 mM H_2SO_4 were dried at 120 °C for 24 h and noted as chemically carbonized nanofibers (CC-CD-NF).

Second method: partial chemical dehydration and pyrolysis of electrospun HPβCD nanofibers

Chemical dehydration process was limited by reducing the acid concentration to obtain partially dehydrated HPβCD nanofibers. The procedure of chemical dehydration mentioned above was repeated by using 10 μM H_2SO_4 and refluxed for approximately 72 h instead of 24 h followed by washing with water to remove the residues of untreated fibers and dried at 120 °C for 24 h. The light yellowish-gray colored nanofibrous mat with approximately 20% of initial fibers was obtained which is referred as partially chemical carbonized HPβCD nanofibers (PCC-CD-NF). The PCC-CD-NF mat was placed inside the tubular furnace (Thermcraft, model number: XST 3-0-18-1V) and pyrolyzed at 800 °C for 3 h with the 5 °C min^{-1} under argon flow at the rate of 100 sccm. Prior to heating, an argon gas was purged inside the furnace tube to replace air with inert argon

atmosphere for 45 min. The CNF synthesized after pyrolysis were referred as carbonized nanofibers based on HPβCD nanofibers (C-CD-NF).

Characterization

The scanning electron microscopy (SEM, FEI Quanta 200 FEG, 10 kV) was used for the morphological investigation of the samples. Prior to SEM imaging, the samples were sputtered with gold (~ 10 nm) in order to eliminate the possible charging. An average of 50 fibers diameter was used for estimating the distribution of the nanofiber diameters by the ImageJ software. X-ray photoelectron spectrometer (XPS, Thermo K-alpha) was used for gathering the information from the samples on the chemical bonding by the survey (2 scans) and high resolution (50 scans; pass energy, 30 eV, step size, 0.1 eV and spot size 400 μm). The presence of crystalline and/or amorphous state of the samples was investigated by PANalytical X-ray powder diffractometer [XRD, CuKα radiation (λ = 1.54 Å)]. The surface area and pore size distribution of samples were analyzed from N_2 adsorption isotherms (77 K) at a relative pressure of 0.995 using multi-point analysis [Brunauer–Emmet–Teller (BET), Quantachrome AutosorbiQ gas sorption analyzer]. The total pore volume and average radius diameter were calculated by the density functional theory (DFT) method. Before N_2 adsorption isotherms, the samples were degassed at 120 °C for 12 h under high vacuum. The Raman spectra for the samples were recorded by WITec alpha 300 confocal Raman at 3 different spots.

Results and discussion

An effect of chemical and thermal treatment on the morphology of HPβCD nanofibers was studied by SEM images (Fig. 1a–e). The chemical treatment on the HPβCD nanofibers (Fig. 1a, b) with the 0.6 mM H_2SO_4 concentration affects their fiber morphology and forms the CNF with fused structure. However, after reducing the H_2SO_4 concentration from 0.6 mM to 10 μM during the chemical treatment of HPβCD nanofibers, it clearly shows that the fiber structure remains intact with noticeable diameter reduction from 1.19 ± 0.33 μm (HPβCD, inset Fig. 1a1) to 650 ± 150 nm (PCC-CD-NF, inset Fig. 1c1). Thus, it is proving the importance of the H_2SO_4 concentration used in the chemical treatment on the morphology of nanofibers. It is expected because the rate of dehydration in the HPβCD nanofibers depends on the H_2SO_4 concentration. The 0.6 mM H_2SO_4 chemical treatment can deform the chemical structure of HPβCD during the process of dehydration, and partial dissolution of HPβCD nanofibers results in the fused nanofibrous structure (Fig. 1b). When the concentration of H_2SO_4 is reduced to 10 μM, partial decomposition of the top layer of HPβCD nanofibers reduces the diameter of nanofibers, keeping its fibrous structure intact. These PCC-CD-NF after pyrolysis further reduce the nanofiber diameters with the unbroken nanofiber structure which results in the CNF having an average diameter of 380 ± 150 nm (C-CD-NF, inset Fig. 1d1). Unlike CC-CD-NF, the fused nanofibrous structure was not observed in the PCC-CD-NF. To confirm the importance of partial chemical treatment in the CNF formation, the pyrolysis of HPβCD nanofibers was carried out excluding the chemical treatment which results in the total decomposition of fibrous morphology with the formation of char (Fig. 1e). This result of char formation by the direct pyrolysis of HPβCD nanofibers is in good agreement with the previous report on the thermal decomposition of CD [42].

The degree of carbon formation was determined by the Raman spectra (Fig. 2a). The Raman spectrum of HPβCD nanofibers is presented in Fig. 2a (red line). The peaks at ca. 430 cm^{-1} (the skeletal modes of α-1,4 linkage), 800 to 1500 cm^{-1}, 3000 cm^{-1} (CH stretching of hydroxypropyl group), and 3100–3600 cm^{-1} (OH stretching) resemble with the HPβCD Raman spectra reported earlier [45, 46]. The emergence of new graphitic carbon peak (G bands at 1580 cm^{-1}) in addition to the disordered carbon peak (D band at 1330 cm^{-1}) validates the conversion of HPβCD nanofibers into the carbon of the CC-CD-NF (Fig. 2a, blue spectrum) and C-CD-NF (Fig. 2a, black spectrum). Furthermore, an absence of Raman bands of HPβCD nanofibers (at ca. 430 cm^{-1}, 800 to 1500 cm^{-1}, 3000 cm^{-1}, and 3100–3600 cm^{-1}) in the CC-CD-NF and C-CD-NF verifies total carbonization of HPβCD nanofibers. The Raman bands observed in the HPβCD nanofibers are also present in the PCC-CD-NF (with reduced peak intensities) proving that HPβCD nanofibers were partially decomposed and not dehydrated like CC-CD-NF [40]. In addition, the presence of humps at the G band along with the peaks of HPβCD nanofibers substantiates the partial

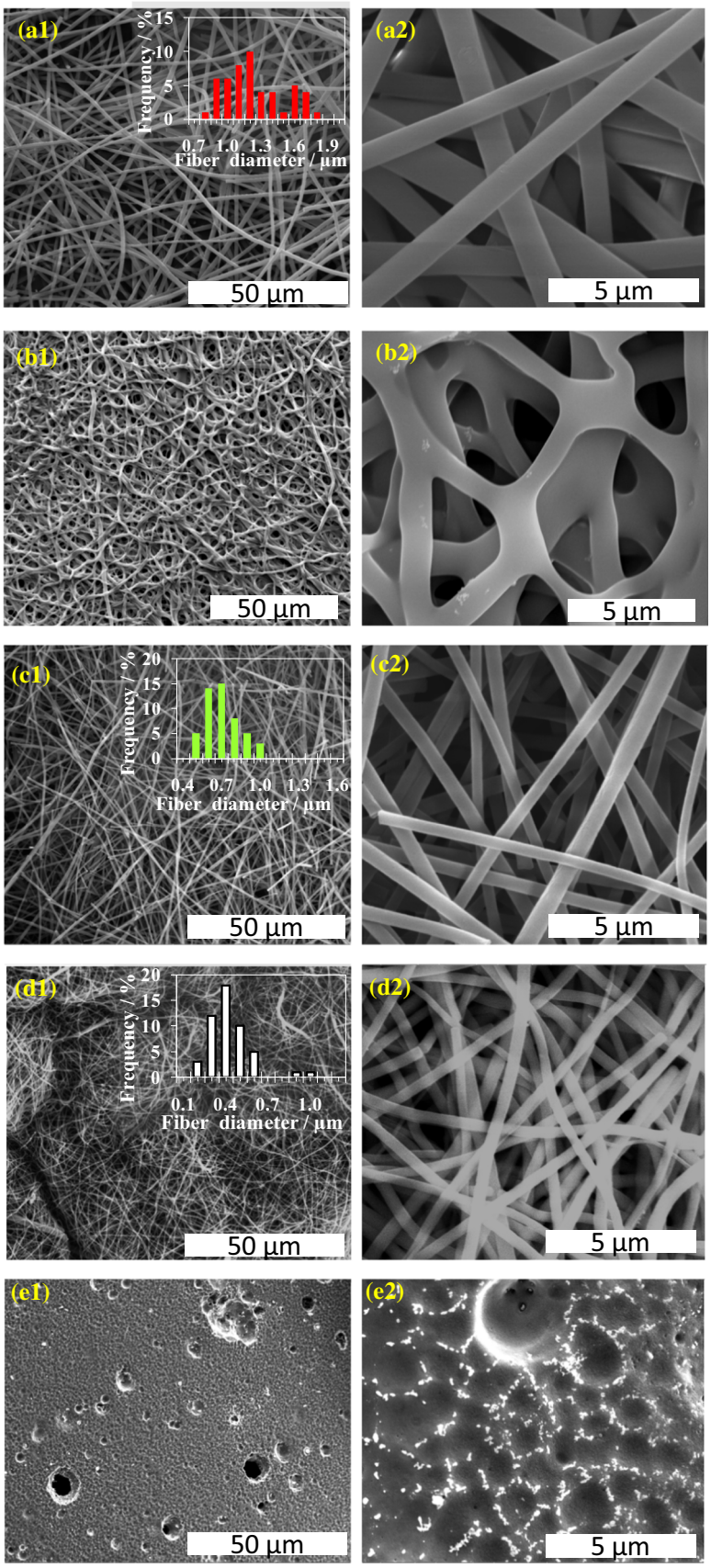

Figure 1 Representative SEM images of **a** HPβCD nanofibers, **b** CC-CD-NF, **c** PCC-CD-NF, **d** C-CD-NF, and **e** char, at the low magnification (1) and high magnification (2). The average nanofiber diameter distribution plotted in the insets for **a1** HPβCD nanofibers, **c1** PCC-CD-NF, and **d1** C-CD-NF.

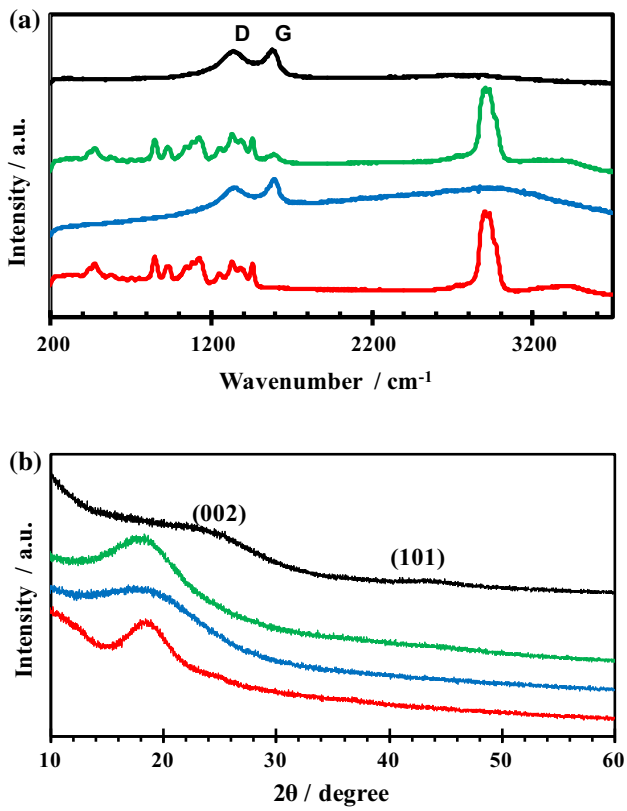

Figure 2 **a** Raman and **b** XRD spectra of HPβCD nanofibers (red line), CC-CD-NF (blue line), PCC-CD-NF (green line), and C-CD-NF (black line).

carbonization (Fig. 2a, green line). This G band is absent in the HPβCD nanofibers while the intensity of this peak increased in the order of PCC-CD-NF < CC-CD-NF = C-CD-NF. Thus, we can conclude that chemical treatment with 10 μM H_2SO_4 initiates graphitic carbon formation which increases by increasing its concentration. Furthermore, upon pyrolysis of PCC-CD-NF, Raman bands of HPβCD nanofibers disappear and only D and G bands remained in the C-CD-NF. It is worth to focus on the intensities of the OH stretching peak (3100–3600 cm^{-1}) in these Raman spectra for HPβCD nanofiber, CC-CD-NF, PCC-CD-NF, and C-CD-NF which has the trend HPβCD nanofibers > PCC-CD-NF > CC-CD-NF > C-CD-NF (almost negligible). It also proves that OH groups are removed from the HPβCD nanofiber surface by the chemical as well as pyrolysis process by the dehydration. The I_D:I_G ratios of the D and G peak intensities for CC-CD-NF and C-CD-NF are 0.84 and 0.97, respectively. Since the G band intensities were almost identical in the CC-CD-NF and C-CD-NF, the difference in the I_D:I_G ratio was due to the increase in the disordered carbon during the pyrolysis. Another possibility of intense G band than the D band in the CC-CD-NF can be related to the lowest size of graphitic plane basal dimension [40, 47].

The crystal structure analyses were performed by XRD, and the diffraction patterns of the samples are plotted in Fig. 2b. As per the earlier studies, HPβCD nanofibers (Fig. 2b, red spectrum) are amorphous having a very broad halo diffraction pattern centered at $2\theta = 19°$ [45]. After chemical treatment with the 0.6 mM H_2SO_4, CC-CD-NF (Fig. 2b, blue spectrum) have broadened this peak as a result of the sum of HPβCD nanofibers amorphous peak and turbostratic carbon ($2\theta \sim 26°$, 002 plane). Furthermore, an absence of a peak at $2\theta \sim 43°$ (101 plane) proved the low value of graphitic plane basal dimension which is in agreement with the Raman spectra, authenticating the amorphous nature of the CC-CD-NF. XRD pattern of PCC-CD-NF (Fig. 2b, green spectrum) has $2\theta \sim 19°$; however, full width half maxima (FWHM) value is higher than HPβCD nanofibers. This broadening of the peak can be referred to the degree of increase in the amorphous nature of PCC-CD-NF than the pristine HPβCD nanofibers. The C-CD-NF (Fig. 2b, black spectrum) clearly present two broad peaks at $2\theta \sim 26°$ and $\sim 43°$ corresponding to 002 and 10 planes of the turbostratic carbon which is further evidence of carbonization of HPβCD nanofibers.

The chemical compositions and atomic binding energies of carbon and oxygen for the nanofibers were analyzed by the XPS (Fig. 3). The atomic percentage of carbon and oxygen in the HPβCD nanofibers (Fig. 3a1), PCC-CD-NF (Fig. 3b1), CC-CD-NF (Fig. 3c1), and C-CD-NF (Fig. 3d1) were C: 62.6% O: 37.4%; C: 63.2% O: 36.8%; C: 75% O: 25%; and C: 94.2% O: 5.8%, respectively. The decrease in the oxygen atomic percentage in the PCC-CD-NF and CC-CD-NF can be assigned to loss of oxygen during the dehydration of HPβCD nanofibers (mainly from the OH group) by the chemical treatment. As the concentration of H_2SO_4 was increased from 10 μM to 0.6 mM, oxygen percent decreases from 33.6 to 25%. The pyrolysis of PCC-CD-NF may remove amorphous carbon, CO and CO_2 (generated during the pyrolysis) which further reduced the oxygen content in the C-CD-NF than the PCC-CD-NF. The removal of these functional groups results in the reduced diameter of C-CD-NF than the PCC-CD-NF and the

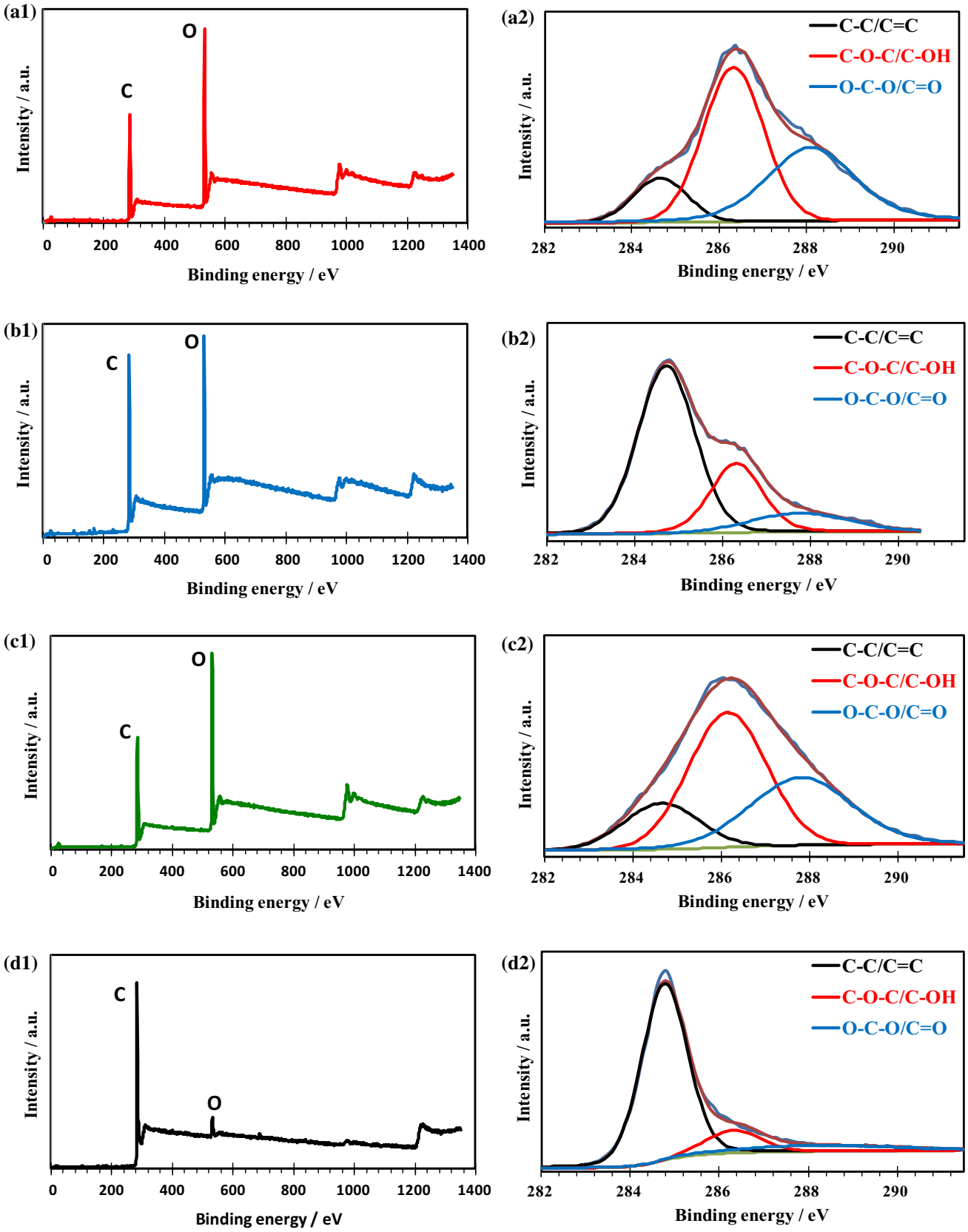

Figure 3 (1) XPS survey and (2) high-resolution carbon XPS of **a** HPβCD nanofibers, **b** CC-CD-NF, **c** PCC-CD-NF, and **d** C-CD-NF.

HPβCD nanofibers. According to the reported carbon and oxygen binding energies, the high-resolution carbon spectra of HPβCD nanofibers, PCC-CD-NF, CC-CD-NF, and C-CD-NF were deconvoluted into three major peaks at the 284.8, 286.2, and 288.0 ± 0.2 eV corresponding to C–C/C=C, C–O–C/C–OH, and O–C–O/C=O (Fig. 3a2–d2) [48, 49]. To reveal an effect of the decomposition process of the HPβCD nanofibers, the ratio of carbon (i.e., C–C/C=C) to the oxidized carbon (i.e., C–O–C/C–OH and O–C–O/C=O) is estimated. It follows the order of HPβCD nanofibers < PCC-CD-NF < CC-CD-NF < C-CD-NF. It shows that the carbon percentage in the CC-CD-NF has increased as the concentration of the H_2SO_4 increased (from 10 μM to 0.6 mM). Furthermore, pyrolysis process has further removed the oxidized carbon in the C-CD-NF than the chemically dehydrated PCC-CD-NF and CC-CD-NF.

The BET analysis (Fig. 4) indicates the N_2 adsorption and desorption curve which follows the type IV isotherm. The DFT (slit pore, NLDFT equilibrium model, at relative pressure $P/Po = 0.995$) is used for the pore volume and diameter measurements (Fig. 4, insets). The total surface area, total pore volume, and average pore diameter of HPβCD nanofibers, CC-CD-NF, PCC-CD-NF, and C-CD-NF are summarized in Table 1. The surface area of HPβCD nanofibers reduced according to the concentration of H_2SO_4 used in the chemical treatment. It is expected due to the blocking of pores as a result of dehydration [40]. Furthermore, the pores in the CC-CD-NF and C-CD-NF were mesopores with the surface area of 5.9 $m^2\ g^{-1}$ and 52.5 $m^2\ g^{-1}$, respectively. Pyrolysis of PCC-CD-NF might have open the blocked pores formed during the dehydration as well as the consequence of some thermal decomposition of PCC-CD-NF which can increase the surface area of C-CD-NF.

The surface area of C-CD-NF is close to the carbon fibers (~ 60 $m^2\ g^{-1}$) obtained from PAN fibers. In addition, turbostratic nature of C-CD-NF creates more edges or in other words defects which can be beneficial in deposition of numerous nanoparticles for catalytic purpose also for the gas storage like hydrogen [50]. Thus, C-CD-NF can be useful as a support in catalytic reactions like oxygen reduction,

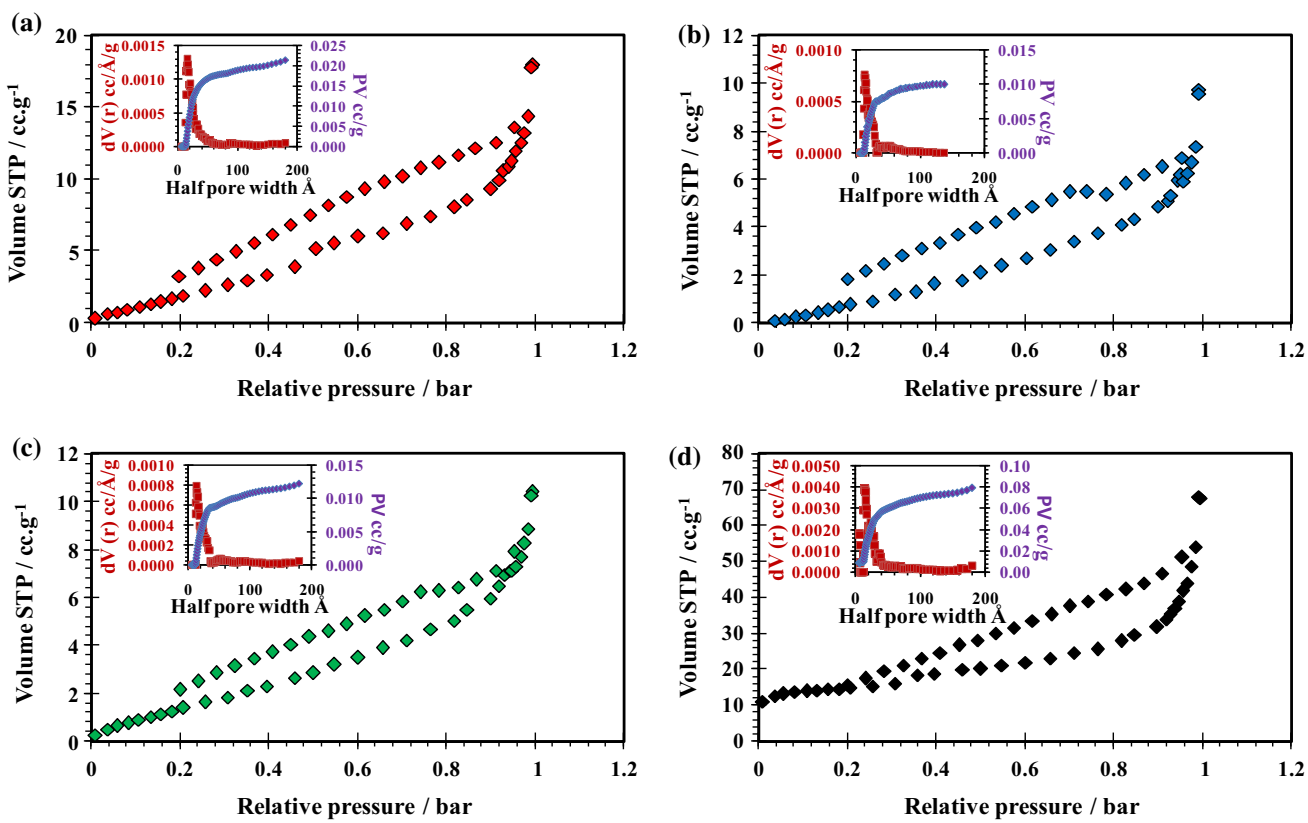

Figure 4 N_2 adsorption–desorption plots obtained for **a** HPβCD nanofibers, **b** CC-CD-NF, **c** PCC-CD-NF, and **d** C-CD-NF. The inset shows the DFT plots for the cumulative pore volume (PV) and dV with respect to half pore width for the respective samples.

Table 1 Porosity characteristics of HPβCD nanofibers, CC-CD-NF, PCC-CD-NF, and C-CD-NF

Sample	Surface area (m^2 g^{-1})	Pore volume (cm^3 g^{-1})	Pore radius (Å)
HPβCD nanofibers	8.6	0.027	64
CC-CD-NF	5.9	0.014	49
PCC-CD-NF	6.7	0.016	48
C-CD-NF	52.5	0.104	39

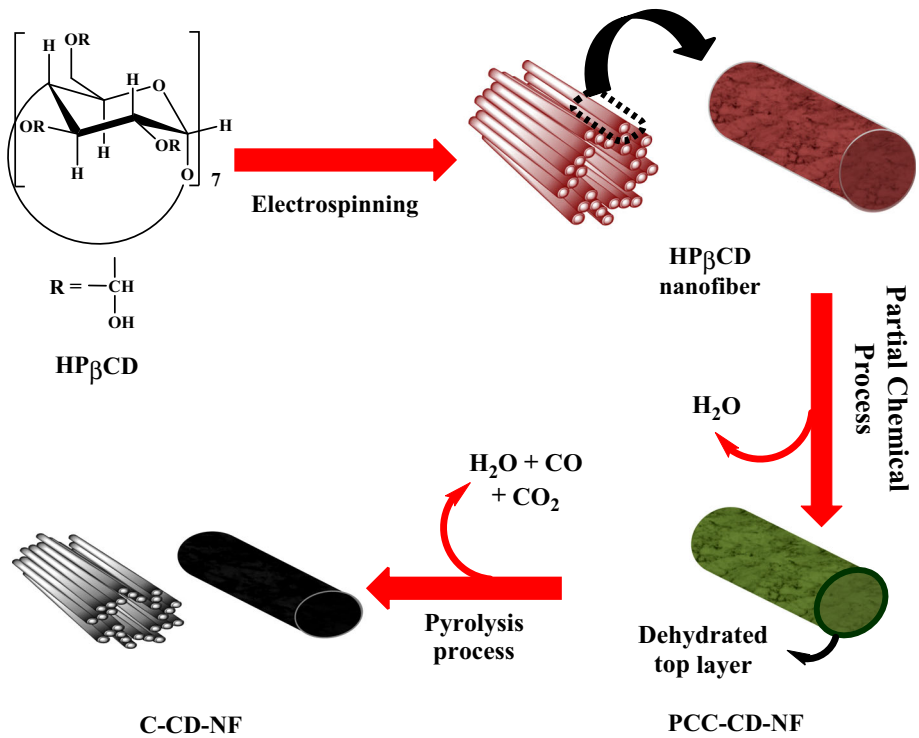

Figure 5 Schematic representation of C-CD-NF formation from the electrospun HPβCD nanofibers.

water splitting, energy storage material, hydrogen storage, sensors and it can be also useful for water filtration to remove toxic elements [13, 20].

Proposed mechanism of CNF synthesis from the electrospun HPβCD nanofibers

Due to the presence of the Raman bands of HPβCD nanofibers and carbon in the PCC-CD-NF (i.e., 10 μM H_2SO_4 treated electrospun HPβCD nanofibers), it is clear that it produced a partially dehydrated layer on top of the HPβCD nanofibers. These results were further confirmed by the slight decrease in the oxygen content of the PCC-CD-NF (33.6%) than the HPβCD nanofibers (37.4%). The electrospun HPβCD nanofibers are water soluble while PCC-CD-NF become insoluble due to surface dehydration. Thus, we predict that partial dehydration by low concentrated acid treatment (10 μM H_2SO_4) forms the thin coating of hydrophobic layers on the HPβCD nanofibers by removal of some hydroxyl groups. On the contrary, a high concentration of H_2SO_4 treatment (0.6 mM) on the electrospun HPβCD nanofibers results in more dehydration than PCC-CD-NF. Furthermore, chances of partial dissolution of some HPβCD nanofibers might be possible in the presence of high acid concentration which results in the fused CC-CD-NF.

The OH group in the CD plays a vital role during the thermal decomposition process by dehydration through depolymerization and cross-linking. Thus, replacing it by attaching another polymer or other functional groups like the tosyl group has been tried [41]. Selection of proper replacement is required to change the thermal decomposition of CD; therefore, as reported earlier, tosyl group can increase the CDF decomposition while amino groups do not show any

significant change [41]. Any functional group which makes hydrogen bond may lead to such decomposition [41, 43]. Therefore, partial chemical treatment to reduce the OH groups is an important step for successful retaining fibrous morphology during the pyrolysis. The importance of this step is further validated by the pyrolysis of electrospun HPβCD nanofibers which results in the char formation with the total destruction of fibrous morphology. The OH group or formation of water during the pyrolysis of electrospun HPβCD nanofibers (i.e., without chemical treatment) may easily oxidize the carbon to form CO and CO_2 at elevated temperature which results in the total destruction of nanofibers [51, 52]. Thus, the overall mechanism of CNF formation from the electrospun HPβCD nanofibers by the combination of partial chemical and pyrolysis process is proposed in Fig. 5.

Conclusions

The electrospun polymer-free HPβCD nanofibers were successfully converted to CNF without breaking the fibrous morphology with the combination of partial chemical dehydration and pyrolysis process. The dehydration of electrospun HPβCD nanofibers with the 0.6 mM H_2SO_4 leads to fused CNF while direct pyrolysis results in a char formation. The effect of each treatment on the HPβCD nanofiber morphology was analyzed by SEM, which shows that fibrous structure remains intact after the combination of partial chemical and pyrolysis treatment yielding CNF having fiber diameter of 380 ± 150 nm. Carbon formation in the CC-CD-NF and C-CD-NF is confirmed by the presence of only D and G bands of Raman spectra (with almost negligible peaks of HPβCD nanofibers) while PCC-CD-NF has both D and G bands along with the bands of HPβCD nanofibers (low intensity). The XRD of HPβCD nanofibers ($2\theta \sim 19°$) shifts to broad peak at $2\theta \sim 26°$ for CC-CD-NF (slight hump) and C-CD-NF, while PCC-CD-NF does show significant change. The chemical composition by XPS shows the percentage of carbon atom in the order of HPβCD nanofibers < PCC-CD-NF < CC-CD-NF < C-CD-NF and oxygen atom have the trend of HPβCD nanofibers > PCC-CD-NF > CC-CD-NF > C-CD-NF. The surface area of C-CD-NF is similar to the carbon fibers obtained from PAN fibers. Therefore, controlled OH removal from the electrospun polymer-free HPβCD nanofibers found to be the crucial process during the CNF synthesis. Reducing the hydroxyl functional groups from the top layer of HPβCD nanofibers by the partial dehydration process is found to be the key step for CNF formation based on the electrospun HPβCD nanofibers. Although the synthesis process is quite long, fiber structure remains intact after pyrolysis without formation of char; this process can be further useful for the fabrication of novel carbon structures with the inclusion complex of cyclodextrins.

Compliance with ethical standards

Conflict of interest The authors declare that they have no conflict of interest.

References

[1] Hirsch A (2010) The era of carbon allotropes. Nat Mater 9:868–871

[2] Sharon M, Mishra N, Patil B, Mewada A, Gurung R, Sharon M (2015) Conversion of polypropylene to two-dimensional graphene, one-dimensional carbon nano tubes and zero-dimensional C-dots, all exhibiting typical sp^2-hexagonal carbon rings. IET Circuits Devices Syst 9:59–66

[3] Maniecki T, Shtyka O, Mierczynski P, Ciesielski R, Czylkowska A, Leyko J et al (2018) Carbon nanotubes: properties, synthesis, and application. Fibre Chem 50:297–300

[4] Castro Neto AH, Guinea F, Peres NMR, Novoselov KS, Geim AK (2009) The electronic properties of graphene. Rev Mod Phys 81:109–162

[5] Brozena AH, Kim M, Powell LR, Wang Y (2019) Controlling the optical properties of carbon nanotubes with organic colour-centre quantum defects. Rev. Chem, Nat. https://doi.org/10.1038/s41570-019-0103-5

[6] Balandin AA (2011) Thermal properties of graphene and nanostructured carbon materials. Nat Mater 10:569–581

[7] Goze C, Vaccarini L, Henrard L, Bernier P, Hernandez E, Rubio A (1999) Elastic and mechanical properties of carbon nanotubes. Synth Met 103:2500–2501

[8] Candelaria SL, Shao Y, Zhou W, Li X, Xiao J, Zhanget JG et al (2012) Nanostructured carbon for energy storage and conversion. Nano Energy 1:195–220

[9] Pech D, Brunet M, Durou H, Huang P, Mochalin V, Gogotsi Y et al (2010) Ultrahigh-power micrometre-sized supercapacitors based on onion-like carbon. Nat Nanotechnol 5:651–654

[10] Qureshi A, Kang WP, Davidson JL, Gurbuz Y (2009) Review on carbon-derived, solid-state, micro and nano

sensors for electrochemical sensing applications. Diam Relat Mater 18:1401–1420

[11] Yang W, Thordarson P, Gooding JJ, Ringer SP, Braet F (2007) Carbon nanotubes for biological and biomedical applications. Nanotechnology 18:1–12

[12] Street KW, Miyoshi K, Vander Wal RL (2007) Application of carbon based nano-materials to aeronautics and space lubrication. In: Erdemir A, Martin J-M (eds) Superlubricity. Elsevier, Amsterdam, pp 311–340

[13] Mauter MS, Elimelech M (2008) Critical review environmental applications of carbon-based nanomaterials. Am Chem Soc 42:5843–5859

[14] Huang X (2009) Fabrication and properties of carbon fibers. Materials (Basel) 2:2369–2403

[15] Newcomb BA (2016) Processing, structure, and properties of carbon fibers. Compos Part A 91:262–282

[16] Zhang D, Bhat GS (1994) Carbon fibers from polyethylene-based precursors. Mater Manuf Process 9:221–235

[17] Stanzione J, La Scala J (2016) Sustainable polymers and polymer science: dedicated to the life and work of Richard P. Wool. J Appl Polym Sci 133:1–2

[18] Hiremath N, Mays J, Bhat G (2017) Recent developments in carbon fibers and carbon nanotube-based fibers: a review. Polym Rev 57:339–368

[19] Uyar T, Kny E (2017) Electrospun materials for tissue engineering and biomedical applications: research, design and commercialization, Woodhead Publishing Series in Biomaterials, 1st edn. Elsevier, London

[20] Khalily MA, Patil B, Yilmaz E, Uyar T (2019) Atomic layer deposition of Co_3O_4 nanocrystals on N-doped electrospun carbon nanofibers for oxygen reduction and oxygen evolution reactions. Nanoscale Adv 1:1224–1231

[21] Yang Y, Centrone A, Chen L, Simeon F, Alan Hatton T, Rutledge GC (2011) Highly porous electrospun polyvinylidene fluoride (PVDF)-based carbon fiber. Carbon 49:3395–3403

[22] Patil B, Satilmis B, Khalily MA, Uyar T (2019) Atomic layer deposition of $NiOOH/Ni(OH)_2$ on PIM-1-based N-doped carbon nanofibers for electrochemical water splitting in alkaline medium. Chemsuschem 12:1469–1477

[23] Ruiz-Rosas R, Bedia J, Lallave M, Loscertales IG, Barrero A, Rodríguez-Mirasol J et al (2010) The production of submicron diameter carbon fibers by the electrospinning of lignin. Carbon 48:696–705

[24] Zhang B, Kang F, Tarascon JM, Kim JK (2016) Recent advances in electrospun carbon nanofibers and their application in electrochemical energy storage. Prog Mater Sci 76:319–380

[25] Kumar M, Hietala M, Oksman K (2019) Lignin-based electrospun carbon nanofibers. Front Mater 6:1–6

[26] Szejtli J (1998) Introduction and general overview of cyclodextrin chemistry. Chem Rev 98:1743–1754

[27] Szente L (2002) Highly soluble cyclodextrin derivatives: chemistry, properties, and trends in development. Adv Drug Deliv Rev 36:17–28

[28] Topuz F, Uyar T (2018) Influence of hydrogen-bonding additives on electrospinning of cyclodextrin nanofibers. ACS Omega 3:18311–18322

[29] Manasco JL, Saquing CD, Tang C, Khan SA (2012) Cyclodextrin fibers via polymer-free electrospinning. RSC Adv 2:3778–3784

[30] Celebioglu A, Uyar T (2012) Electrospinning of nanofibers from non-polymeric systems: polymer-free nanofibers from cyclodextrin derivatives. Nanoscale 4:621–631

[31] Celebioglu A, Uyar T (2019) Electrospinning of cyclodextrins: hydroxypropyl-alpha-cyclodextrin nanofibers. J Mater Sci. https://doi.org/10.1007/s10853-019-03983-x

[32] Celebioglu A, Uyar T (2010) Cyclodextrin nanofibers by electrospinning. Chem Commun 46:6903–6905

[33] Vass P, Démuth B, Farkas A, Hirsch E, Szabó E, Nagyi B et al (2019) Continuous alternative to freeze drying: manufacturing of cyclodextrin-based reconstitution powder from aqueous solution using scaled-up electrospinning. J Control Release 298:120–127

[34] Yıldız ZI, Uyar T (2019) Fast-dissolving electrospun nanofibrous films of paracetamol/cyclodextrin inclusion complexes. Appl Surf Sci 492:626–633

[35] Yıldız ZI, Celebioglu A, Uyar T (2017) Polymer-free electrospun nanofibers from sulfobutyl ether7-beta-cyclodextrin (SBE7-β-CD) inclusion complex with sulfisoxazole fast-dissolving and enhanced water-solubility of sulfisoxazole. Int J Pharm 531:550–558

[36] Kida T, Sato S, Yoshida H, Teragaki A, Akashi M (2014) 1,1,1,3,3,3-Hexafluoro-2-propanol (HFIP) as a novel and effective solvent to facilely prepare cyclodextrin-assembled materials. Chem Commun 50:14245–14248

[37] Celebioglu A, Uyar T (2013) Electrospinning of nanofibers from non-polymeric systems: electrospun nanofibers from native cyclodextrins. J Colloid Interface Sci 404:1–7

[38] Ahn Y, Kang Y, Ku M, Yang Y-H, Jung S, Kim H (2013) Preparation of β-cyclodextrin fiber using electrospinning. RSC Adv 3:14983–14987

[39] Online VA (2013) Electrospun gamma-cyclodextrin (γ-CD) nanofibers for the entrapment of volatile organic compounds. RSC Adv 1:22891–22895

[40] Jaouadi M, Hbaieb S, Guedidi H, Reinert L, Amdouni N, Duclaux L (2017) Preparation and characterization of carbons from β-cyclodextrin dehydration and from olive pomace activation and their application for boron adsorption. J Saudi Chem Soc 21:822–829

[41] Trotta F, Zanetti M, Camino G (2000) Thermal degradation of cyclodextrins. Polym Degrad Stab 69:373–379
[42] Zhu C, Krumm C, Facas GG, Neurock M, Dauenhauer PJ (2017) Energetics of cellulose and cyclodextrin glycosidic bond cleavage. React Chem Eng 2:201–214
[43] Zanetti M, Anceschi A, Magnacca G, Spezzati G, Caldera F, Rosi GP et al (2016) Micro porous carbon spheres from cyclodextrin nanosponges. Microporous Mesoporous Mater 235:178–184
[44] Cecone C, Zanetti M, Anceschi A, Caldera F, Trotta F, Bracco P (2019) Microfibers of microporous carbon obtained from the pyrolysis of electrospun β-cyclodextrin pyromellitic dianhydride nanosponges. Polym Degrad Stab 161:277–282
[45] Celebioglu A, Topuz F, Yildiz ZI, Uyar T (2019) One-step green synthesis of antibacterial silver nanoparticles embedded in electrospun cyclodextrin nanofibers. Carbohydr Polym 207:471–479
[46] Yang X, Ke W, Zi P, Liu F, Yu L (2008) Detecting and identifying the complexation of nimodipine with hydroxypropyl-β-cyclodextrin present in tablets by Raman spectroscopy. J Pharm Sci 97:2702–2719
[47] Ferrari AC, Robertson J (2000) Interpretation of Raman spectra of disordered and amorphous carbon. Phys Rev B 61:14095–14107
[48] Yang Z, Ji H (2013) 2-Hydroxypropyl-β-cyclodextrin polymer as a mimetic enzyme for mediated synthesis of benzaldehyde in water. ACS Sustain Chem Eng 1:1172–1179
[49] Uyar T, Havelund R, Nur Y, Hacaloglu J, Besenbacher F, Kingshott P (2009) Molecular filters based on cyclodextrin functionalized electrospun fibers. J Membr Sci 332:129–137
[50] Wu HC, Li YY, Sakoda A (2010) Synthesis and hydrogen storage capacity of exfoliated turbostratic carbon nanofibers. Int J Hydrogen Energy 35:4123–4130
[51] Jung I, Dikin D, Park S, Cai W, Mielke SL, Ruoff RS (2008) Effect of water vapor on electrical properties of individual reduced graphene oxide sheets. J Phys Chem C 112:20264–20268
[52] Mettler MS, Mushrif SH, Paulsen AD, Javadekar AD, Vlachos DG, Dauenhauer PJ (2012) Revealing pyrolysis chemistry for biofuels production: conversion of cellulose to furans and small oxygenates. Energy Environ Sci 5:5414–5424